Quantum Effects in the Nonlinear Response of Graphene Plasmons – Supporting Information –

Joel D. Cox,[1] Iván Silveiro,[1] and F. Javier García de Abajo[1,2]

[1]*ICFO-Institut de Ciencies Fotoniques, The Barcelona Institute of Science and Technology, 08860 Castelldefels (Barcelona), Spain*
[2]*ICREA-Institució Catalana de Recerca i Estudis Avançats, Passeig Lluís Companys 23, 08010 Barcelona, Spain*

(Dated: January 5, 2016)

We elaborate on the classical method used to simulate the linear and nonlinear optical response associated with plasmon resonances in graphene nanostructures, with emphasis on the derivation of Eqs. (1-4) in Methods. We also discuss and explore the influence of temperature and interband transitions on the optical response of nanographenes, and provide frequency-dependent values of the nonlinear refractive index and nonlinear absorption coefficient for graphene nanoribbons. Finally, we give additional details pertaining to the fast-Fourier transform method used to expedite calculations for graphene nanoislands.

Contents

I. CLASSICAL ELECTROSTATIC THEORY FOR NANOSTRUCTURED GRAPHENE

We consider a graphene nanostructure with a characteristic size D, corresponding to the width of a nanoribbon or the side length of an equilateral triangle, that is much less than the wavelength of the incident illumination, for which the electric field is given by $\mathbf{E}^{\rm ext} = E_0\hat{\mathbf{e}}\left(\mathrm{e}^{-\mathrm{i}\omega t} + \text{c.c.}\right)$, where $\hat{\mathbf{e}}$ is the polarization unit vector. We quantify the linear and nonlinear optical response of a finite nanostructure by the $n^{\rm th}$-order dipole induced along $\hat{\mathbf{e}}$ oscillating at harmonic s of the excitation frequency ω, for which the polarizability is given by

$$\alpha^{(n)}_{s\omega}(\omega) = \frac{1}{(E_0)^n}\int d^2\mathbf{R}\,(\hat{\mathbf{e}}\cdot\mathbf{R})\,\rho^{\mathrm{ind},(n)}_{s\omega}(\mathbf{R},\omega), \tag{1}$$

where the induced charge density is obtained from the surface currents $\mathbf{j}^{(n)}_{s\omega}(\mathbf{R},\omega)$ using the continuity equation,

$$\rho^{\mathrm{ind},(n)}_{s\omega}(\mathbf{R},\omega) = -\frac{\mathrm{i}}{s\omega}\nabla_{\mathbf{R}}\cdot\mathbf{j}^{(n)}_{s\omega}(\mathbf{R},\omega), \tag{2}$$

and $\mathbf{R} = (x, y)$ are 2-D coordinate vectors in the x-y plane.

For the linear optical response (taking $n = s = 1$ in the above expressions), the surface current is $\mathbf{j}^{(1)}_{\omega}(\mathbf{R},\omega) = \sigma^{(1)}_{\omega}(\mathbf{R},\omega)\mathbf{E}(\mathbf{R},\omega)$, where $\sigma^{(1)}_{\omega}(\mathbf{R},\omega)$ is the linear conductivity of graphene (see Methods) and $\mathbf{E}(\mathbf{R},\omega) = -\nabla_{\mathbf{R}}\phi(\mathbf{R},\omega)$ is the total electric field acting on the graphene nanostructure due to the self-consistent potential ϕ, which is given in the electrostatic approximation by [1]

$$\phi(\mathbf{R},\omega) = \phi^{\rm ext}(\mathbf{R},\omega) + \frac{\mathrm{i}}{\omega}\int\frac{d^2\mathbf{R}'}{|\mathbf{R}-\mathbf{R}'|}\nabla_{\mathbf{R}'}\cdot\sigma^{(1)}_{\omega}(\mathbf{R}',\omega)\nabla_{\mathbf{R}'}\phi(\mathbf{R}',\omega). \tag{3}$$

Following the method of Ref. [1], we assume that the linear conductivity can be separated as $\sigma_\omega^{(1)}(\mathbf{R},\omega) = f(\mathbf{R})\sigma_\omega^{(1)}(\omega)$, where the occupation factor $f(\mathbf{R})$ is 1 within the graphene structure and zero everywhere else, and we express Eq. (2) in terms of a reduced 2-D coordinate vector $\vec{\theta} = \mathbf{R}/D$ as

$$\rho_\omega^{\mathrm{ind},(1)}(\vec{\theta},\omega) = -\frac{\eta_\omega^{(1)}}{D}\nabla_{\vec{\theta}}\cdot\sqrt{f(\vec{\theta})}\,\vec{\varepsilon}(\vec{\theta},\omega)/D. \tag{4}$$

In obtaining the above expression we have defined $\eta_{s\omega}^{(n)} = \mathrm{i}\sigma_{s\omega}^{(n)}(\omega)/s\omega D$ and introduced the normalized electric field $\vec{\varepsilon}(\vec{\theta},\omega) = -\sqrt{f(\vec{\theta})}\nabla_{\vec{\theta}}\phi(\vec{\theta},\omega)$, which is expanded in a complete set of eigenmodes $\vec{\varepsilon}_j$ with real eigenvalues $1/\eta_j$ as [1]

$$\vec{\varepsilon}(\vec{\theta},\omega) = \sum_j \frac{c_j}{1-\eta_\omega^{(1)}/\eta_j}\vec{\varepsilon}_j(\vec{\theta}), \tag{5}$$

where the expansion coefficients are

$$c_j = \int d^2\vec{\theta}\vec{\varepsilon}_j(\vec{\theta})\cdot\vec{\varepsilon}^{\,\mathrm{ext}}(\vec{\theta},\omega) = DE_0\hat{\mathbf{e}}\cdot\int d^2\vec{\theta}\sqrt{f(\vec{\theta})}\vec{\varepsilon}_j(\vec{\theta}), \tag{6}$$

and the eigenmodes are orthogonal, *i.e.*,

$$\vec{\varepsilon}_j(\vec{\theta}) = \int d^2\vec{\theta}\vec{\varepsilon}_j(\vec{\theta})\cdot\vec{\varepsilon}_j(\vec{\theta}) = \delta_{jj'}. \tag{7}$$

Now, assuming that the optical response is dominated by the lowest-order dipolar mode [the $j=1$ term in Eq. (5)], the induced charge density given in Eq. (4) becomes

$$\rho_\omega^{\mathrm{ind},(1)}(\vec{\theta},\omega) = -\frac{\eta_\omega^{(1)}}{D}\frac{c_1}{1-\eta_\omega^{(1)}/\eta_1}\nabla_{\vec{\theta}}\cdot\sqrt{f(\vec{\theta})}\vec{\varepsilon}_1(\vec{\theta}). \tag{8}$$

We then express Eq. (1) in terms of normalized coordinates $\vec{\theta}$ and use Eq. (8) to write the linear polarizability as

$$\alpha_\omega^{(1)}(\omega) = \frac{\eta_\omega^{(1)}\xi_1^2 D^3}{1-\eta_\omega^{(1)}/\eta_1}, \tag{9}$$

where we have defined

$$\xi_1 = \hat{\mathbf{e}}\cdot\int d^2\vec{\theta}\vec{\theta}\nabla_{\vec{\theta}}\cdot\sqrt{f(\vec{\theta})}\vec{\varepsilon}_1(\vec{\theta}) = -\hat{\mathbf{e}}\cdot\int d^2\vec{\theta}\sqrt{f(\vec{\theta})}\vec{\varepsilon}_1(\vec{\theta}). \tag{10}$$

Moving back to $\mathbf{R}$ space, we write $\xi_1 = -\hat{\mathbf{e}}\cdot\int_S d^2\mathbf{R}\,\vec{\varepsilon}_1(\mathbf{R})/D^2$, as given in Methods of the main paper, by using the function $f(\mathbf{R})$ to restrict the integration to the surface of the graphene nanostructure, S, while Eq. (7) guarantees that $\int_S d^2\mathbf{R}|\vec{\varepsilon}_1(\mathbf{R})|^2 = D^2$.

To describe the nonlinear response associated with second-harmonic generation (SHG), we express the second-harmonic current as [2]

$$j_{2\omega,i}^{(2)}(\mathbf{R},\omega) = \sigma_{2\omega}^{(2)}(\mathbf{R},\omega)\sum_{jkl}\boldsymbol{\Delta}_{ijkl}^{(2)}E_j(\mathbf{R},\omega)\partial_k E_l(\mathbf{R},\omega), \tag{11}$$

where we assume that the nonlinear conductivity can be written as $\sigma_{2\omega}^{(2)}(\mathbf{R},\omega) = f(\mathbf{R})\sigma_{2\omega}^{(2)}(\omega)$, and we have isolated its tensorial part, $\boldsymbol{\Delta}_{ijkl}^{(2)} = 5\delta_{ij}\delta_{kl}/3 - \delta_{ik}\delta_{jl} + \delta_{il}\delta_{jk}/3$. We then express Eq. (2), for $n=s=2$, in reduced coordinates as

$$\rho_{2\omega}^{\mathrm{ind},(2)}(\vec{\theta},\omega) = -\frac{\eta_{2\omega}^{(2)}}{D^3}\sum_{ijkl}\partial_{\vec{\theta},i}\left[\boldsymbol{\Delta}_{ijkl}^{(2)}\sqrt{f(\vec{\theta})}\varepsilon_j(\vec{\theta},\omega)\partial_{\vec{\theta},k}\frac{1}{\sqrt{f(\vec{\theta})}}\varepsilon_l(\vec{\theta},\omega)\right]. \tag{12}$$

Keeping the total electric field to linear order, we again use only the $j=1$ term in Eq. (5) and write

$$\rho_{2\omega}^{\mathrm{ind},(2)}(\vec{\theta},\omega) = -\frac{\eta_{2\omega}^{(2)}}{D^3}\frac{c_1^2}{\left(1-\eta_\omega^{(1)}/\eta_1\right)^2}\sum_{ijkl}\partial_{\vec{\theta},i}\left[\boldsymbol{\Delta}_{ijkl}^{(2)}\sqrt{f(\vec{\theta})}\varepsilon_{1,j}(\vec{\theta})\partial_{\vec{\theta},k}\frac{1}{\sqrt{f(\vec{\theta})}}\varepsilon_{1,l}(\vec{\theta})\right]. \tag{13}$$

Using the above expression in Eq. (1), expressed in terms of $\vec{\theta}$, then yields the nonlinear polarizability for SHG,

$$\alpha^{(2)}_{2\omega}(\omega) = \frac{\eta^{(2)}_{2\omega}\xi_1^2\zeta^{(2)}_{2\omega}D^2}{\left(1-\eta^{(1)}_{\omega}/\eta_1\right)^2}, \tag{14}$$

where we introduce the dimensionless parameter

$$\zeta^{(2)}_{2\omega} = -\int d^2\vec{\theta}\left(\vec{\theta}\cdot\hat{\mathbf{e}}\right)\sum_{ijkl}\partial_{\vec{\theta},i}\left[\mathbf{\Delta}^{(2)}_{ijkl}\sqrt{f(\vec{\theta})}\varepsilon_{1,j}(\vec{\theta})\partial_{\vec{\theta},k}\frac{\varepsilon_{1,l}(\vec{\theta})}{\sqrt{f(\vec{\theta})}}\right] = \sum_{ijkl}\hat{\mathbf{e}}_i\mathbf{\Delta}^{(2)}_{ijkl}\int d^2\vec{\theta}\sqrt{f(\vec{\theta})}\varepsilon_{1,j}(\vec{\theta})\partial_{\vec{\theta},k}\frac{\varepsilon_{1,l}(\vec{\theta})}{\sqrt{f(\vec{\theta})}}. \tag{15}$$

Note that $\varepsilon_{1,i}(\vec{\theta})/\sqrt{f(\vec{\theta})}$ is proportional to the physical electric field associated with the dipolar plasmon mode, and therefore is continuous across the graphene edge, even in the limit where $f(\vec{\theta})$ jumps from 1 to 0 at the edge itself; the leading factor of $\sqrt{f(\vec{\theta})}$ then limits the integration in the above expression to the region occupied by the graphene, S. By moving to $\mathbf{R}$ space, and considering (without loss of generality) the response along the x-direction, *i.e.*, for $\hat{\mathbf{e}}_x$, we may express $\zeta^{(2)}_{2\omega}$ in the form

$$\zeta^{(2)}_{2\omega} = \frac{1}{D}\int_S d^2\mathbf{R}\left\{\varepsilon_{1,x}(\mathbf{R})\left[\frac{\partial}{\partial x}\varepsilon_{1,x}(\mathbf{R}) + \frac{5}{3}\frac{\partial}{\partial y}\varepsilon_{1,y}(\mathbf{R})\right] + \varepsilon_{1,y}(\mathbf{R})\left[\frac{1}{3}\frac{\partial}{\partial y}\varepsilon_{1,x}(\mathbf{R}) - \frac{\partial}{\partial x}\varepsilon_{1,y}(\mathbf{R})\right]\right\}, \tag{16}$$

which corresponds to the expression provided in Methods.

The extension to third-order nonlinearities follows straightforwardly: For third-harmonic generation (THG), we start with the third-order surface current

$$j^{(3)}_{3\omega,i}(\mathbf{R},\omega) = \sigma^{(3)}_{3\omega}(\mathbf{R},\omega)\sum_{jkl}\mathbf{\Delta}^{(3)}_{ijkl}E_j(\mathbf{R},\omega)E_k(\mathbf{R},\omega)E_l(\mathbf{R},\omega), \tag{17}$$

where the tensor part is $\mathbf{\Delta}^{(3)}_{ijkl} = \left(\delta_{ij}\delta_{kl}+\delta_{ik}\delta_{jl}+\delta_{il}\delta_{jk}\right)/3$. We isolate the spatial dependence of the third-order conductivity according to $\sigma^{(3)}_{3\omega}(\mathbf{R},\omega) = f(\mathbf{R})^2\sigma^{(3)}_{3\omega}(\omega)$, and so Eq. (2) (for $n=s=3$) becomes

$$\rho^{\mathrm{ind},(3)}_{3\omega}(\vec{\theta},\omega) = -\frac{\eta^{(3)}_{3\omega}}{D^3}\sum_{ijkl}\partial_{\vec{\theta},i}\left[\mathbf{\Delta}^{(3)}_{ijkl}\sqrt{f(\vec{\theta})}\varepsilon_j(\vec{\theta},\omega)\varepsilon_k(\vec{\theta},\omega)\varepsilon_l(\vec{\theta},\omega)\right]. \tag{18}$$

Using Eq. (5), we find that

$$\rho^{\mathrm{ind},(3)}_{3\omega}(\vec{\theta},\omega) = -\frac{\eta^{(3)}_{3\omega}}{D^3}\frac{c_1^3}{\left(1-\eta^{(1)}_{\omega}/\eta_1\right)^3}\sum_{ijkl}\partial_{\vec{\theta},i}\left[\mathbf{\Delta}^{(3)}_{ijkl}\sqrt{f(\vec{\theta})}\varepsilon_{1,j}(\vec{\theta})\varepsilon_{1,k}(\vec{\theta})\varepsilon_{1,l}(\vec{\theta})\right], \tag{19}$$

from which Eq. (1) provides the nonlinear polarizability corresponding to THG,

$$\alpha^{(3)}_{3\omega}(\omega) = \frac{\eta^{(3)}_{3\omega}\xi_1^3\zeta^{(3)}_{3\omega}D^3}{\left(1-\eta^{(1)}_{\omega}/\eta_1\right)^3}, \tag{20}$$

where

$$\zeta^{(3)}_{3\omega} = \int d^2\vec{\theta}\left(\vec{\theta}\cdot\hat{\mathbf{e}}\right)\sum_{ijkl}\partial_{\vec{\theta},i}\left[\mathbf{\Delta}^{(3)}_{ijkl}\sqrt{f(\vec{\theta})}\varepsilon_{1,j}(\vec{\theta})\varepsilon_{1,k}(\vec{\theta})\varepsilon_{1,l}(\vec{\theta})\right] = -\sum_{ijkl}\hat{\mathbf{e}}_i\mathbf{\Delta}^{(3)}_{ijkl}\int d^2\vec{\theta}\sqrt{f(\vec{\theta})}\varepsilon_{1,j}(\vec{\theta})\varepsilon_{1,k}(\vec{\theta})\varepsilon_{1,l}(\vec{\theta}). \tag{21}$$

The above expression for the dimensionless parameter $\zeta^{(3)}_{3\omega}$ is simplified by moving to $\mathbf{R}$ coordinates and using the property $f(\mathbf{R}) = 1$ for $\mathbf{R}\in S$, and is zero otherwise, to write

$$\zeta^{(3)}_{3\omega} = -\frac{1}{D^2}\hat{\mathbf{e}}\cdot\int_S d^2\mathbf{R}\,\vec{\varepsilon}_1(\mathbf{R})\cdot\vec{\varepsilon}_1(\mathbf{R})\,\vec{\varepsilon}_1(\mathbf{R}), \tag{22}$$

corresponding to the expression provided in Methods.

In an analogous manner, the nonlinear polarizability corresponding to the Kerr nonlinearity [Eq. (1) for $n = 3$, $s = 1$] is obtained from the third-order surface current

$$j^{(3)}_{\omega,i}(\mathbf{R},\omega) = \sigma^{(3)}_{3\omega}(\mathbf{R},\omega)\sum_{jkl}\mathbf{\Delta}^{(3)}_{ijkl}E_j(\mathbf{R},\omega)E^*_k(\mathbf{R},\omega)E_l(\mathbf{R},\omega) \tag{23}$$

as

$$\alpha^{(3)}_{\omega}(\omega) = \frac{\eta^{(3)}_{\omega}\xi_1^3\zeta^{(3)}_{\omega}D^3}{\left|1-\eta^{(1)}_{\omega}/\eta_1\right|^2\left(1-\eta^{(1)}_{\omega}/\eta_1\right)} \tag{24}$$

where

$$\zeta^{(3)}_{\omega} = \int d^2\vec{\theta}\left(\vec{\theta}\cdot\hat{\mathbf{e}}\right)\sum_{ijkl}\partial_{\vec{\theta},i}\left[\mathbf{\Delta}^{(3)}_{ijkl}\sqrt{f(\vec{\theta})}\varepsilon_{1,j}(\vec{\theta})\varepsilon^*_{1,k}(\vec{\theta})\varepsilon_{1,l}(\vec{\theta})\right] = -\sum_{ijkl}\hat{\mathbf{e}}_i\mathbf{\Delta}^{(3)}_{ijkl}\int d^2\vec{\theta}\sqrt{f(\vec{\theta})}\varepsilon_{1,j}(\vec{\theta})\varepsilon^*_{1,k}(\vec{\theta})\varepsilon_{1,l}(\vec{\theta}). \tag{25}$$

After performing the summation in the above expression, we obtain

$$\zeta^{(3)}_{\omega} = -\frac{1}{D^2}\hat{\mathbf{e}}\cdot\int_S d^2\mathbf{R}\left\{\frac{2}{3}\left|\vec{\varepsilon}_1(\mathbf{R})\right|^2\vec{\varepsilon}_1(\mathbf{R}) + \frac{1}{3}\vec{\varepsilon}_1(\mathbf{R})\cdot\vec{\varepsilon}_1(\mathbf{R})\left[\vec{\varepsilon}_1(\mathbf{R})\right]^*\right\}, \tag{26}$$

which coincides with the expression provided in Methods.

II. TEMPERATURE DEPENDENCE OF THE OPTICAL RESPONSE

Through iterative solution of the Boltzmann transport equation (in the local limit),

$$\frac{\partial f_{\mathbf{k}}(\mathbf{r},t)}{\partial t} - \frac{e}{\hbar}\mathbf{E}\cdot\nabla_{\mathbf{k}}f_{\mathbf{k}}(\mathbf{r},t) = -\frac{1}{\tau}\left[f_{\mathbf{k}}(\mathbf{r},t) - f^0_{\mathbf{k}}\right], \tag{27}$$

we consider an electric field $\mathbf{E}(t) = \mathbf{E}_\omega(\mathrm{e}^{-\mathrm{i}\omega t} + \mathrm{e}^{\mathrm{i}\omega t})$ and find that, to first-order,

$$\sigma^{(1)}_{\omega}(\omega) = \mathrm{i}\frac{e^2}{\pi\hbar^2}\frac{F^{(1)}_{\mathbf{k}}}{\omega + \mathrm{i}\tau^{-1}}, \tag{28}$$

with

$$F^{(1)}_{\mathbf{k}} = \int_{-\infty}^{\infty} d\varepsilon_k\left|\varepsilon_k\right|\frac{\partial f^0_{\mathbf{k}}}{\partial\varepsilon_k} = E_F + 2k_BT\log\left(1+\mathrm{e}^{-E_F/k_BT}\right),$$

so that Eq. (28) leads to Eq. (5) of the main text in the $T \to 0$ limit. Actually, the linear result is virtually unchanged by considering $T = 300\,\mathrm{K}$, for which we find $F^{(1)}_{\mathbf{k}} \simeq E_F$ for the Fermi energies considered in this work, *i.e.* for $0.2 \leq E_F/\mathrm{eV} \leq 2.0$. At third-order, we obtain expressions for the local intraband conductivity of graphene as

$$\sigma^{(3)}_{s\omega}(\omega) = -\mathrm{i}\frac{e^4v_F^2}{\pi^2\hbar^2}\frac{-sF^{(3)}_{\mathbf{k}}}{D_{s\omega}}, \tag{29}$$

where

$$F^{(3)}_{\mathbf{k}} = \int_{-\infty}^{\infty} d\varepsilon_k\left(\frac{-1}{|\varepsilon_k|}\frac{\partial f^0_{\mathbf{k}}}{\partial\varepsilon_k} + \frac{\partial^2 f^0_{\mathbf{k}}}{\partial\varepsilon_k^2} + |\varepsilon_k|\frac{\partial^3 f^0_{\mathbf{k}}}{\partial\varepsilon_k^3}\right), \tag{30}$$

and $D_{3\omega} = (\omega+\mathrm{i}\tau^{-1})(2\omega+\mathrm{i}\tau^{-1})(3\omega+\mathrm{i}\tau^{-1})$ for THG ($s = 3$) or $D_\omega = (\omega+\mathrm{i}\tau^{-1})(2\omega+\mathrm{i}\tau^{-1})(-\omega+\mathrm{i}\tau^{-1})$ for the Kerr nonlinearity ($s = 1$). Now, at zero temperature, we have $\partial f^0_{\mathbf{k}}/\partial\varepsilon_k = -\delta\left(E_F - \varepsilon_k\right)$, and Eq. (30) reduces to $F^{(3)}_{\mathbf{k}} = -3\pi/4$, after having used the general relation

$$\int dx\frac{\partial^n f(x)}{\partial x^n}\delta(a-x) = (-1)^n\left.\frac{\partial^n f(x)}{\partial x^n}\right|_{x=a}. \tag{31}$$

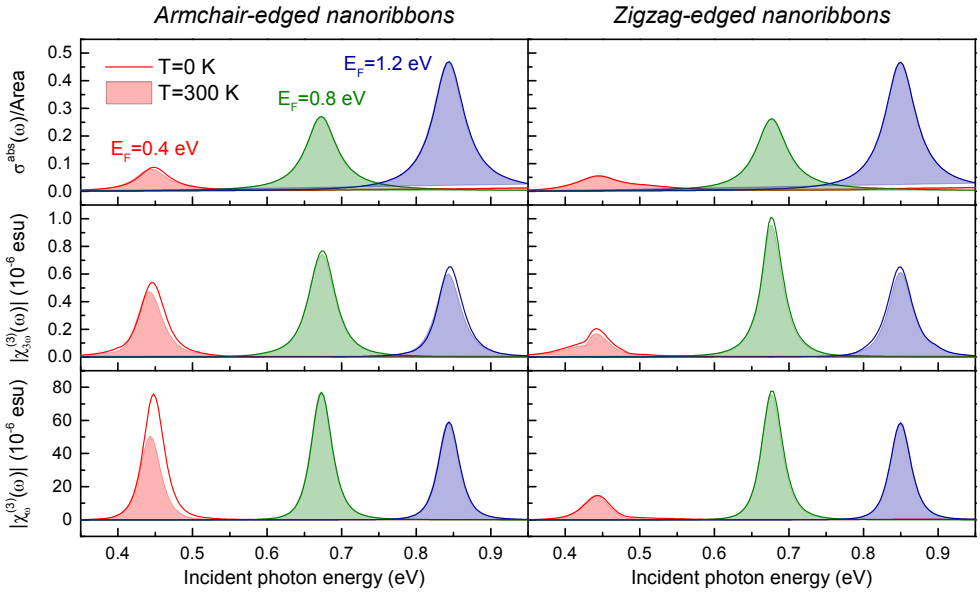

FIG. S1: **Temperature dependence of the nonlinear optical response in nanoribbons.** We show spectra for the linear absorption cross-section (upper panels), along with the nonlinear polarizabilities corresponding to THG (middle panels), and the Kerr nonlinearity (lower panels) for $\sim 10\,\mathrm{nm}$ armchair- (left panels) and zigzag-edged (right panels) nanoribbons at zero temperature (filled curves) and for $T = 300\,\mathrm{K}$ (regular curves). Different Fermi energies are considered here, as indicated by the color-coded numerical values in the upper-left panel.

Thus, we recover

$$\sigma^{(3)}_{3\omega}(\omega) = \frac{3\mathrm{i}e^4 v_F^2}{4\pi\hbar^2 E_F}\frac{1}{(\omega+\mathrm{i}\tau^{-1})(2\omega+\mathrm{i}\tau^{-1})(3\omega+\mathrm{i}\tau^{-1})} \tag{32}$$

and

$$\sigma^{(3)}_{\omega}(\omega) = \frac{9\mathrm{i}e^4 v_F^2}{4\pi\hbar^2 E_F}\frac{1}{(\omega+\mathrm{i}\tau^{-1})(-\omega+\mathrm{i}\tau^{-1})(2\omega+\mathrm{i}\tau^{-1})},$$

corresponding to Eqs. (9) and (10) in Methods, and in agreement with the result of Ref. [3]. These third-order expressions differ in multiplicative factors from those reported in a previous study [4], where the phenomenological decay is introduced in the Fourier integrals; if in Eq. (27) we had instead defined $\mathbf{E}(t) = \int_{-\infty}^{\infty} d\omega \mathbf{E}_\omega \mathrm{e}^{-i\omega t + t/\tau}$, we would recover the purely intraband contributions to the third-order currents obtained from Ref. [4]:

$$\sigma^{(3)}_{3\omega}(\omega) = \frac{\mathrm{i}e^4 v_F^2}{8\pi\hbar^2 E_F}\frac{1}{(\omega+\mathrm{i}\tau^{-1})^3} \tag{33}$$

and

$$\sigma^{(3)}_{\omega}(\omega) = \frac{3\mathrm{i}e^4 v_F^2}{8\pi\hbar^2 E_F}\frac{1}{(\omega+\mathrm{i}\tau^{-1})^2(-\omega+\mathrm{i}\tau^{-1})}.$$

For non-zero temperatures, Eq. (30) becomes

$$F^{(3)}_{\mathbf{k}} = \frac{-3\pi}{4k_BT}\left\{\int_{-\infty}^{\infty}\frac{d\varepsilon_k}{|\varepsilon_k|}\frac{\mathrm{e}^{(\varepsilon_k-E_F)/k_BT}}{\left[\mathrm{e}^{(\varepsilon_k-E_F)/k_BT}+1\right]^2} + \frac{2\mathrm{e}^{-E_F/k_BT}}{(\mathrm{e}^{-E_F/k_BT}+1)^2}\right\}. \tag{34}$$

Note that the integrand in the first term above has a singularity at $\varepsilon_k = 0$, and so $F^{(3)}_{\mathbf{k}}$ diverges. This suggests that the perturbation theory (up to third order) is inadequate for dealing with finite temperatures, in the same way it fails as $E_F \to 0$ (consider the $1/E_F$ dependence of $\sigma^{(3)}_{s\omega}$). However, we expect that the $T = 0$ description of the third-order, purely intraband conductivities should also describe the $T = 300\,\mathrm{K}$ case reasonably well, considering the negligible change in the linear response [see Eq. (28)], as well as those in the nonlinear response for graphene nanoribbons predicted by atomistic simulations (see Fig. S1).

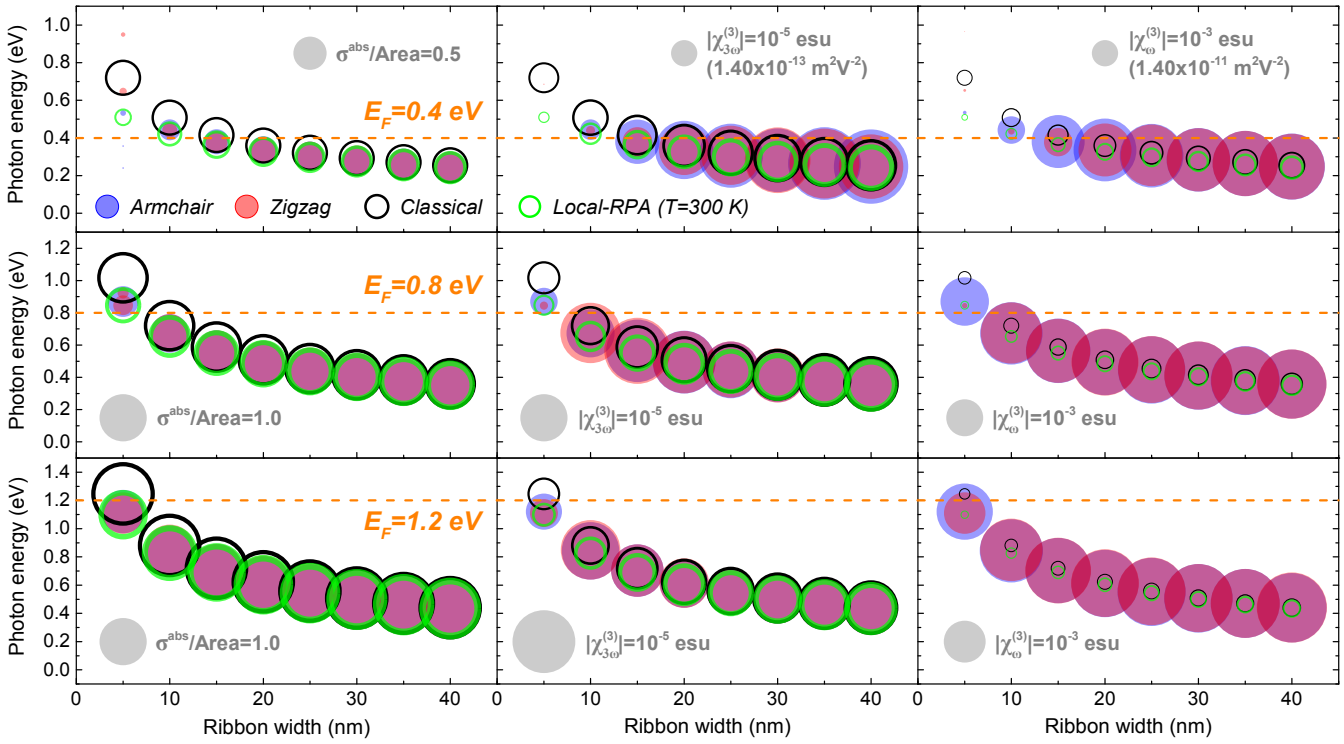

FIG. S2: **Exploring the role of interband transitions in the optical response of nanoribbons.** The symbols indicate the peak maxima for the linear absorption cross-section (left column), as well those for the nonlinear polarizabilities corresponding to THG (central column) and the Kerr nonlinearity (right column), calculated for graphene nanoribbons illuminated by light polarized perpendicular to their direction of translational symmetry. Results are presented for QM calculations of armchair (solid blue circles) and zigzag (solid red circles) ribbons, along with classical simulations for purely intraband contributions in the linear and nonlinear conductivities (open black circles) or including interband contributions in the linear conductivity (open green circles). The peak maxima are proportional to the symbol areas (see grey legends in each panel).

III. INTERBAND CONTRIBUTIONS TO THE NONLINEAR OPTICAL RESPONSE

Computing the full third-order nonlinear optical conductivity of extended graphene, *i.e.*, including contributions from both intraband and interband optical transitions, is presently an area of active study, with various approaches in the literature that apparently yield different results (see for example the work of Cheng et al. in Refs. [5, 6] and by Mikhailov in Ref. [4]). In the present study, we focus primarily on the nonlinear optical response of graphene nanostructures associated with plasmonic exctations, for which only intraband processes contribute significantly to the nonlinear conductivities. Incidentally, it has been argued that interband transitions only become important at energies $\hbar\omega \geq 2E_F$, and even then their effect is orders of magnitude smaller than the contribution of intraband transitions [4].

A relatively simple, straightforward improvement to the classical description of the plasmon-enhanced nonlinear response in nanostructured graphene can be achieved by including the effect of interband optical transitions in the linear response. This is accomplished by using the linear conductivity for graphene obtained from the random-phase approximation in the local limit [7],

$$\sigma_\omega^{(1)}(\omega) = \mathrm{i}\frac{e^2}{\pi\hbar^2}\frac{1}{\omega+\mathrm{i}\tau^{-1}}\left[F_{\mathbf{k}}^{(1)} - \int_{-\infty}^{\infty} d\varepsilon_k \frac{(\varepsilon_k/|\varepsilon_k|)f_{\mathbf{k}}^0(\varepsilon_k)}{1-4\varepsilon_k^2/\left[\hbar^2\left(\omega+\mathrm{i}\tau^{-1}\right)^2\right]}\right]. \tag{35}$$

The linear conductivity enters the factors $\eta_\omega^{(1)}$ in Eqs. (1-4) of Methods, where it accounts for the local field generated by the dipolar plasmon mode of a graphene nanostructure. An accurate treatment of this local field enhancement is arguably more critical than the inclusion of interband optical transitions in the nonlinear conductivities when describing the nonlinear response at plasmon resonances. Indeed, as we show in Fig. S2 for graphene nanoribbons, the peak intensities of the linear and nonlinear response are in better agreement with those predicted in quantum-

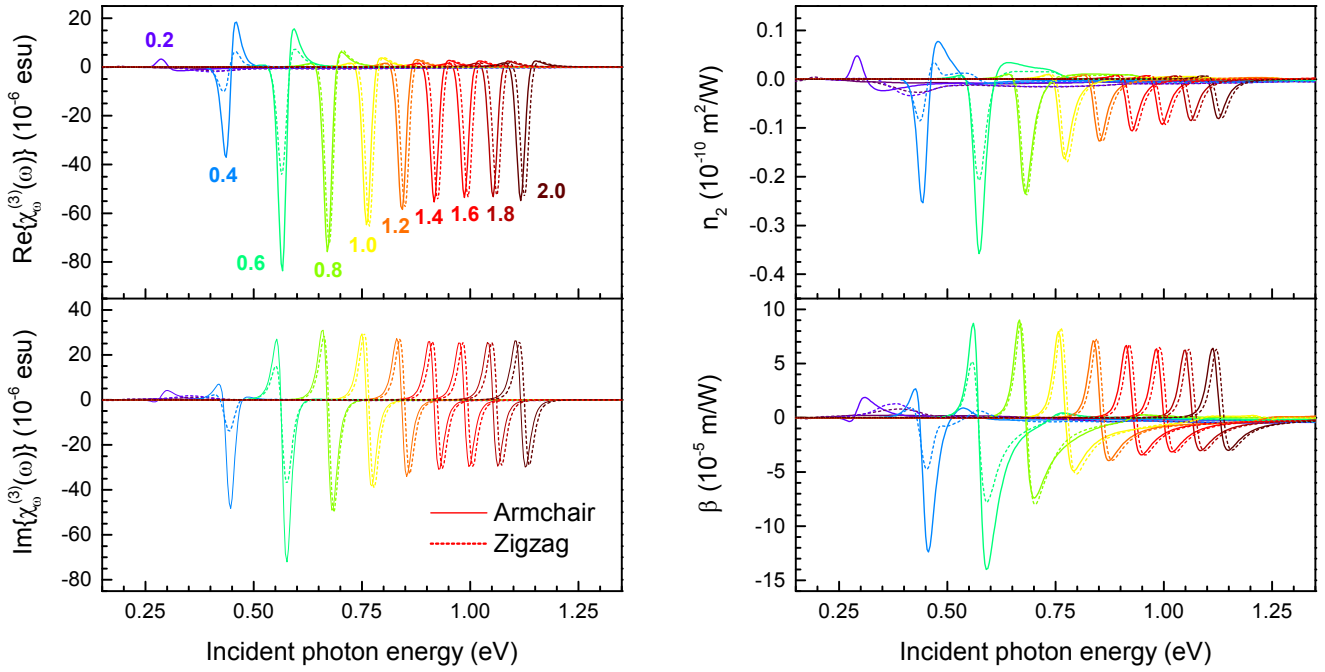

FIG. S3: **Kerr-type nonlinearities in graphene nanoribbons** We present the real and imaginary parts of the third-order nonlinear susceptibilities used to produce Fig. 1d in the main text (left column, in electrostatic units), along with the corresponding values of the nonlinear refractive index, n_2, and the nonlinear absorption coefficient, β (right column, in SI units). Different Fermi energies [color-coded numerical values in (a), eV] are considered, and the ribbon width is $\approx 10\,\text{nm}$.

mechanical simulations when we use Eq. (35) to describe the linear conductivity in graphene, where the most noticeable improvements appear for resonances above or near the Fermi level.

IV. NONLINEAR REFRACTIVE INDEX AND NONLINEAR ABSORPTION

The complex third-order susceptibility oscillating at the fundamental frequency of illumination, $\chi^{(3)}_\omega$, which quantifies what we have referred to here as the Kerr nonlinearity, is related to the nonlinear refractive index n_2 and nonlinear absorption coefficient β of a medium. These quantities are typically what are measured directly in nonlinear optical experiments, from which values for the nonlinear susceptibility are inferred. The relations among a medium's $\chi^{(3)}_\omega$, n_2, and β are provided in Ref. [8] as

$$n_2 = \frac{3}{4\epsilon_0 c\,(n_0^2+k_0^2)}\left(\text{Re}\{\chi^{(3)}_\omega\}+\frac{k_0}{n_0}\text{Im}\{\chi^{(3)}_\omega\}\right) \tag{36}$$

and

$$\beta = \frac{3}{2\epsilon_0 c^2\,(n_0^2+k_0^2)}\left(\text{Im}\{\chi^{(3)}_\omega\}-\frac{k_0}{n_0}\text{Re}\{\chi^{(3)}_\omega\}\right), \tag{37}$$

where $n_0 = \text{Re}\{(1+\chi^{(1)}_\omega)^{1/2}\}$ and $k_0 = \text{Im}\{(1+\chi^{(1)}_\omega)^{1/2}\}$, with all of the above quantities in SI units. The above expressions are intended to properly account for the interplay between the complex first- and third-order susceptibilities in highly-absorbing media [8], and we use them here to show the frequency-dependence of n_2 and β for the $\sim 10\,\text{nm}$ graphene nanoribbons considered in Fig. 1 of the main text.

V. CONVERGENCE OF THE FAST-FOURIER TRANSFORM METHOD FOR NANOISLANDS

Here we describe the nonlinear response for graphene nanotriangles using the perturbative expansion procedure for the single-electron density matrix outlined in Ref. [9]. Following this approach, we compute several noninteracting

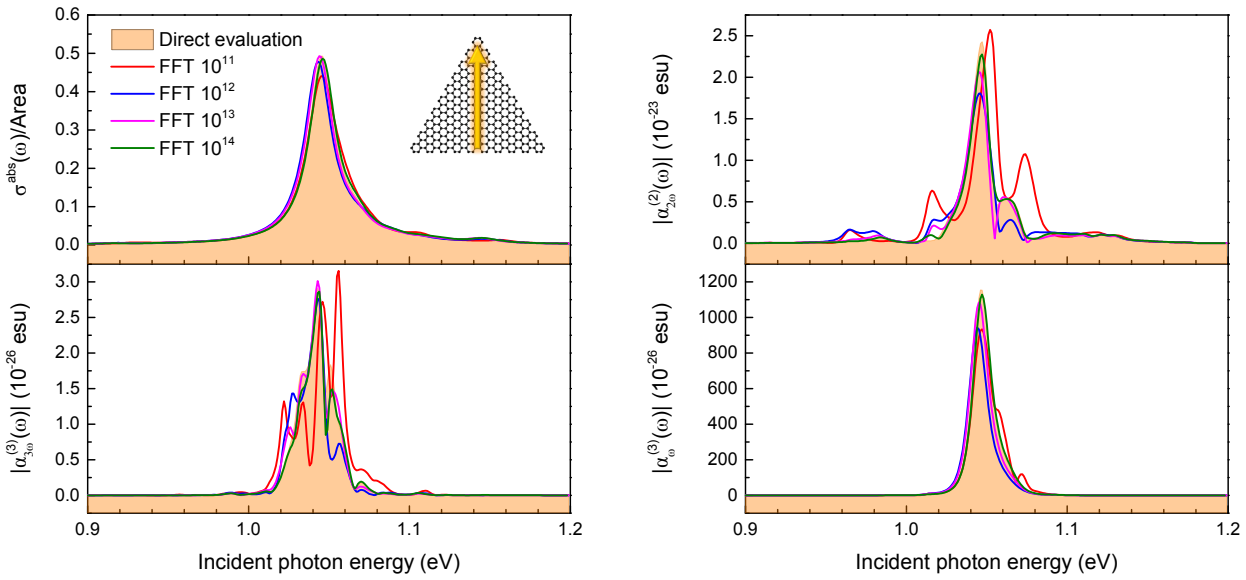

FIG. S4: **Convergence of the FFT method for graphene nanoislands.** We show spectra for the linear absorption cross-section (upper left), along with the nonlinear polarizabilities corresponding to SHG (upper right), THG (lower left), and the Kerr nonlinearity (lower right) for a $\sim 4.4\,$nm, armchair-edged nanotriangle, with light polarized in the graphene plane and perpendicular to one of the triangle sides (see inset in upper-left panel). Results are shown for a simulation in which the RPA susceptibility is evaluated directly (filled curves) along with those computed using the fast-Fourier transform (FFT) method, using the indicated number of frequencies in the Fourier integral.

RPA susceptibilities, $\chi^0_{ll'}(s\omega)$, which have the same form as Eq. (23) of Methods (but lack any wave vector dependence), to obtain the nonlinear polarizabilities for a single structure. To expedite these computations, which require summing $\sim N^4$ terms for each $\chi^0_{ll'}(s\omega)$, N being the number of carbon atoms in a nanoisland, we employ the fast-Fourier transform (FFT) method described in Ref. [10], for which only $\sim N^3$ operations are required. To perform the FFT, a finite grid of N_ω equally-spaced frequencies must be defined, and it is this discretization that determines the convergence of the $\chi^0_{ll'}(s\omega)$ computed using the FFT method with that obtained from a direct summation. In Fig. S4, we show that while the FFT method can provide excellent convergence for $N_\omega = 10^{12}$ frequencies, particularly in the linear response, more satisfactory results for the nonlinear polarizabilities are obtained with 10^{13} frequencies. Note that while this convergence is rather independent of a graphene nanoisland's size, more frequencies are required if the phenomenological relaxation rate is reduced.

[1] García de Abajo, F. J. Multiple Excitation of Confined Graphene Plasmons by Single Free Electrons. *ACS Nano* **2013**, *7*, 11409–11419.

[2] Manzoni, M. T.; Silveiro, I.; García de Abajo, F. J.; Chang, D. E. Second-Order Quantum Nonlinear Optical Processes in Single Graphene Nanostructures and Arrays. *New J. Phys.* **2015**, *17*, 083031.

[3] Peres, N. M. R.; Bludov, Y. V.; Santos, J. E.; Jauho, A.-P.; Vasilevskiy, M. I. Optical Bistability of Graphene in the Terahertz Range. *Phys. Rev. B* **2014**, *90*, 125425.

[4] S. A. Mikhailov, Quantum Theory of the Third-Order Nonlinear Electrodynamic Effects in Graphene, arXiv:1506.00534v2.

[5] Cheng, J. L.; Vermeulen, N.; Sipe, J. E. Third Order Optical Nonlinearity of Graphene. *New J. Phys.* **2014**, *16*, 053104.

[6] Cheng, J. L.; Vermeulen, N.; Sipe, J. E. Third-Order Nonlinearity of Graphene: Effects of Phenomenological Relaxation and Finite Temperature. *Phys. Rev. B* **2015**, *91*, 235320.

[7] García de Abajo, F. J. Graphene Plasmonics: Challenges and Opportunities. *ACS Photon.* **2014**, *1*, 135–152.

[8] del Coso, R.; Solis, J. Relation Between Nonlinear Refractive Index and Third-Order Susceptibility in Absorbing Media *J. Opt. Soc. Am. B* **2004**, *21*, 640–644.

[9] Cox, J. D.; García de Abajo, F. J. Electrically Tunable Nonlinear Plasmonics in Graphene Nanoislands. *Nat. Commun.* **2014**, *5*, 5725.

[10] Thongrattanasiri, S.; Manjavacas, A.; García de Abajo, F. J. Quantum Finite-Size Effects in Graphene Plasmons. *ACS Nano* **2012**, *6*, 1766–1775.